PCCP

PAPER

View Article Online
View Journal | View Issue

Cite this: *Phys. Chem. Chem. Phys.*, 2014, **16**, 19241

Theoretical study of temperature dependence and Rayleigh scattering properties of chloride hydration clusters

Shuai Jiang,[ab] Teng Huang,[ab] Yi-Rong Liu,[ab] Kang-Ming Xu,[ab] Yang Zhang,[ab] Yu-Zhou Lv[ab] and Wei Huang*[ab]

Received 13th June 2014,
Accepted 28th July 2014

DOI: 10.1039/c4cp02618g

www.rsc.org/pccp

$Cl^-(H_2O)_n$ (n = 5–6) clusters were investigated using a basin hopping (BH) method coupled with density functional theory (DFT). Structures, energetics, thermodynamics, and vibrational frequencies were obtained using high level *ab initio* calculations. DF-LMP2 (second-order Møller–Plesset perturbation theory using local and density fitting approximations) with an appropriate basis set were employed for final optimization and frequency calculation, which has been benchmarked in a recent study. The global minimum of $Cl^-(H_2O)_5$ was verified and the new competitive local minimum of $Cl^-(H_2O)_6$ was offered. Considering the increasing complexity of the large system and the high flexibility of the hydrogen bonding environment, Boltzmann averaged Gibbs free energy was provided taking into account the contributions of local minima on the potential energy surface. Finally, the temperature dependence of the conformational population for isomers of $Cl^-(H_2O)_n$ (n = 5–6) and Rayleigh scattering properties of $Cl^-(H_2O)_n$ (n = 1–6) have been investigated systematically for the first time.

Introduction

Halide–water clusters are very important in cluster science because of their unique thermodynamic and spectroscopic properties. Numerous studies have focused on the various aspects of halide–water clusters: structures,[3,4] thermodynamics,[5,6] vibrational spectroscopy,[7–10] photoelectron spectroscopy[11] and charge-transfer-to-solvent (CTTS) energy.[12] In particular, the experimental work of Johnson,[7,8,10] Okumura,[9] and Cheshnovsky[11] provided a great deal of spectroscopic data that yielded critical structural information. Theoretical studies by Kim *et al.*[3,13,14] applied high-level *ab initio* calculations to determine the structures of many halide–water clusters. Recently, Nadykto *et al.*[15] have studied $Cl^{\pm}(H_2O)_n$ system to investigate the sign effect of ion induced nucleation. Besides, inspired by Elm *et al.*[16] who studied the Rayleigh scattering properties of atmospheric pre-nucleation systems and the situation where few literature nowadays focusing on the Rayleigh scattering properties of ionic clusters even though the hydrated electron have been studied,[17,18] the Rayleigh scattering properties of $Cl^-(H_2O)_n$ are given for the first time.

In many calculations, manual searches of structures were performed to obtain information about potential energy surface minima. This approach was less reliable for larger molecular systems with broad minima, which has motivated the use of many global optimization techniques such as genetic algorithms (GA),[19–21] Monte Carlo (MC) simulated annealing,[22] minima hopping[23] and basin hopping (BH).[24] For halide–water systems, Soumya Ganguly Neogi *et al.*[25,26] recently employed GA coupled with density functional theory (DFT) to identify the local and global minima. They demonstrated that this strategy based on GA and DFT was viable for investigating halide solvation systems.

In contrast, BH code has been coupled with quantum chemistry packages such as Dmol[3] (ref. 27) to search for the lowest energy isomers of atomic clusters. The BH approach was highly efficient for many atomic clusters, especially gold clusters,[28–31] boron clusters[32] and doped gold clusters.[33] Furthermore, the ability of BH algorithms coupled with DFT to search for minima on the potential energy surfaces of molecular clusters has been tested for water, methanol and water–methanol clusters, both protonated and unprotonated,[34] as well as the structure and bonding in ionized water clusters.[35] Moreover, a new sampling skill called compressed sampling was recently introduced to BH coupled with DFT and verified by water, nitrate–water and oxalate–water clusters.[36]

Recently, we have utilized BH coupled with DFT to study the structures, energetics, thermodynamics, vertical detachment

[a] *Laboratory of Atmospheric Physico-Chemistry, Anhui Institute of Optics & Fine Mechanics, Chinese Academy of Sciences, Hefei, Anhui 230031, China. E-mail: huangwei6@ustc.edu.cn*
[b] *School of Environmental Science & Optoelectronic Technology, University of Science and Technology of China, Hefei, Anhui 230026, China*

energies (VDEs) and vibrational frequencies of $Cl^-(H_2O)_n$ (n = 1–4) and performed the benchmark work[2] to prove that DF-LMP2[1] is a promising method for geometry optimization and frequency calculations for larger $Cl^-(H_2O)_n$ systems.[2]

In this work, for the first time we determine cluster polarizability and Rayleigh scattering properties including isotropic mean polarizabilities, anisotropic polarizabilities, depolarization ratios and Rayleigh scattering intensities of chloride ion hydration molecular clusters. The formation of hydrogen bonds is expected to lead to an increase in the polarizability anisotropy and therefore a change in the Rayleigh depolarization ratio.[37]

This article has several highlights: (1) BH was coupled with DFT and used to determine the local and global minima by sampling the potential energy surface thoroughly, and a new potential global minimum of $Cl^-(H_2O)_6$ was illustrated; (2) DF-LMP2, which has recently been benchmarked, was applied to perform the final geometry optimization and frequency calculations; (3) the temperature dependence of the conformational population was given in a wide temperature range; (4) to incorporate the contributions of other lower energy isomers besides the global minimum, the Boltzmann averaged Gibbs free energy was determined. (5) The Rayleigh scattering properties of chloride ion hydration systems were investigated for the first time.

Methodology

The potential energy surfaces of $Cl^-(H_2O)_n$ (n = 5–6) were explored using the BH algorithm coupled with DFT implemented in DMol^3 (ref. 27). The number of BH searches was 4 and 5 for $Cl^-(H_2O)_5$ and $Cl^-(H_2O)_6$ clusters, respectively. Every search was performed with 1000 MC steps at 2000 K with randomly generated initial structures. The temperature was a crucial parameter in BH and must be chosen carefully because it affected the tradeoff between the acceptance ratio and the sampling efficiency. At each MC step, all of the molecules were translated and rotated, and the maximum translational and rotational displacements were 2 Å and $\pi/2$, respectively. To prevent the clusters from diverging, we compiled a function to check whether the intermolecular distances exceeded the range defined after the structure perturbation caused by the Monte Carlo sampling. After each MC step, this function automatically determined whether the molecule moved more than 5 Å, which could cause the optimization to fail. If a large divergence occurred, then this function automatically moved the molecules closer together. The atoms in different molecules were not permitted to be closer than 2 Å to prevent the self-consistent field (SCF) calculation from failing to converge.

BLYP/DND implemented in DMol^3 (ref. 27) was employed in the DFT module coupled with BH, where BLYP refers to Becke for the exchange part and Lee, Yang and Parr for the correlation part, and DND means double numerical plus d-functions basis set. Some selected low-lying conformers were then further optimized in the Gaussian 09 suite of programs[38] with the default convergence criteria at the level of BLYP/6-31+G*. Next, further geometry optimization and frequency calculations were performed using DF-LMP2/aug′-cc-pVTZ, where the prime signified that aug-cc-pVTZ was used for Cl and O while cc-pVTZ was used for H, in Molpro 2010.1.[39,40] Because local correlation methods were particularly useful for calculating the weak intermolecular interactions, as the basis set superposition error (BSSE) was reduced significantly,[41,42] we simply utilized DF-LMP2/aug′-cc-pVTZ without counterpoise (CP) corrections[43] to optimize the geometries. The default convergence criteria were defined in the Molpro 2010.1.[39,40] Harmonic vibrational frequency analysis was performed to assure that no imaginary frequencies were present and that, consequently, the structure of interest represented a local or global minimum on the potential energy surface. The zero-point energy (ZPE), the enthalpy and the Gibbs free energy corrections were obtained at 1 atmosphere and at selected temperatures ranging from 50 K to 400 K at 50 K intervals. The structural information (bond lengths) was generated using Chemcraft 1.6 (http://www.chemcraftprog.com).

Based on global minima of $Cl^-(H_2O)_n$ (n = 1–6) calculated at the level of mp2/aug′-cc-pvdz where those of $Cl^-(H_2O)_n$ (n = 1–4) are given from the previous study,[2] the static polarizability and scattering properties of molecular clusters have been calculated. And in order to investigate the relation between the hydrogen bonding network of isomers and optical properties, the Rayleigh light scattering properties of two additional isomers of $Cl^-(H_2O)_5$ are provided. Optical properties as depolarization ratios and Rayleigh scattering intensities for natural, plane-polarized and circular-polarized light are then calculated. For the elastic Rayleigh scattering, the depolarization ratio for natural, plane-polarized and circular-polarized light are given and light scattering intensities and the isotropic mean polarizabilities $\bar{\alpha}$ as well as anisotropic polarizabilities $\Delta\alpha$ are also shown as follows:

$$\sigma_n = \frac{6(\Delta\alpha)^2}{45(\bar{\alpha})^2 + 7(\Delta\alpha)^2} \quad (1)$$

$$\sigma_p = \frac{3(\Delta\alpha)^2}{45(\bar{\alpha})^2 + 4(\Delta\alpha)^2} \quad (2)$$

$$\sigma_c = \frac{\sigma_n}{1 - \sigma_n} \quad (3)$$

$$\Re_n = 45(\bar{\alpha})^2 + 13(\Delta\alpha)^2 \quad (4)$$

$$\Re_{p\perp} = 45(\bar{\alpha})^2 + 7(\Delta\alpha)^2 \quad (5)$$

$$\Re_{p\parallel} = 6(\Delta\alpha)^2 \quad (6)$$

$$\bar{\alpha} = \tfrac{1}{3}(\alpha_{xx} + \alpha_{yy} + \alpha_{zz}) \quad (7)$$

$$(\Delta\alpha)^2 = \tfrac{1}{2}[(\alpha_{xx} - \alpha_{yy})^2 + (\alpha_{yy} - \alpha_{zz})^2 + (\alpha_{zz} - \alpha_{xx})^2] + 3[(\alpha_{xy})^2 + (\alpha_{xz})^2 + (\alpha_{yz})^2] \quad (8)$$

where σ_n, σ_p and σ_c represent the depolarization ratio of natural, plane-polarized and circular-polarized light, respectively, while $\Re_{p\perp}$ and $\Re_{p\parallel}$ are the perpendicular and parallel components of linear polarized light.

Results and discussion

A. Structures and energetics

The representations of these structures were defined using $m + n\_i$ notation. In this notation, "m" and "n" denote the number of water molecules in the first and the second hydration shells of the clusters, respectively. The index "i" was used to distinguish among different structures with the same values of m and n.

In Table 1, the binding energies of the lower energy isomers are shown. The calculated total electronic energies were transformed into binding energies using the following equation:

$$\Delta E_n^i = E_n^i - n \times E_{H_2O} - E_{Cl^-} \quad (9)$$

where n and i indicate the water number in the cluster and the name of an isomer individually; E is the total energy; and E_{H_2O} and E_{Cl^-} are the total energy for H_2O and Cl^-, respectively. Thermodynamic parameters such as the enthalpy and Gibbs free energy were calculated in a similar way.

An overview of all the conformers suggests that the $Cl^-(H_2O)_n$ (n = 5–6) clusters prefer surface solvation, as discussed previously in the literature.[4] For $Cl^-(H_2O)_5$, isomers within 3 kcal mol^{-1} from the global minimum are dominated by isomers with three or four water molecules in the first hydration shell. In addition, from $Cl^-(H_2O)_5$ to $Cl^-(H_2O)_6$, more configurations with five water molecules binding to the chloride ion appear.

Fig. 1 displays the structures optimized with DF-LMP2/aug′-cc-pVTZ for $Cl^-(H_2O)_5$. For the global minimum, some reports in the literature have characterized quite different configurations, as some gave a water ring composed of three molecules[4,44] instead of four[13] as shown in other literature. Comparatively, our predicted global minimum agrees well with the results from Han Myoung Lee *et al.*[13] In addition, the predicted global minimum proposed by Robert W. Gora *et al.*[4] and M. Masamura[44] is similar to 4 + 1_5, which is 8.71 kcal mol^{-1} higher than our predicted global minimum, and R2AA (3 + 2) from Han Myoung *et al.*[13]

Table 1 Binding energies at 0 K (ΔE_e^{0K}), ZPE-corrected binding energies at 0 K (ΔE_0^{0K}), enthalpies at 298.15 K ($\Delta H^{298.15K}$), Gibbs free energy at 298.15 K ($\Delta G^{298.15K}$) for isomers of $Cl^-(H_2O)_5$ (in kcal mol^{-1})

Isomers	ΔE_e^{0K}	ΔE_0^{0K}	$\Delta H^{298.15K}$	$\Delta G^{298.15K}$
4 + 1_1	−69.35	−57.64	−58.50	−36.46
4 + 1_2	−69.07	−57.48	−58.28	−36.37
3 + 2_1	−68.21	−56.57	−57.48	−35.38
3 + 2_2	−68.02	−56.44	−56.75	−36.29
3 + 2_3	−67.98	−56.39	−56.70	−36.22
4 + 1_3	−67.74	−56.45	−57.08	−35.72
4 + 1_4	−67.34	−55.92	−57.19	−34.27
3 + 2_4	−67.33	−55.86	−57.28	−33.88
3 + 2_5	−66.93	−55.86	−56.99	−34.45
4 + 1_5	−66.92	−55.91	−56.90	−34.53
3 + 2_6	−66.86	−55.04	−55.53	−34.68
4 + 1_6	−66.74	−55.76	−56.74	−34.41
3 + 2_7	−66.66	−55.14	−56.61	−33.30
3 + 2_8	−66.63	−55.25	−56.63	−33.48
5 + 0_1	−66.55	−55.18	−56.41	−33.74
3 + 2_9	−66.48	−54.98	−56.44	−33.11
3 + 2_10	−66.31	−55.00	−56.31	−33.32
3 + 2_11	−66.26	−54.83	−55.65	−34.01

The geometries optimized with DF-LMP2/aug′-cc-pVTZ for $Cl^-(H_2O)_6$ are displayed in Fig. 2. For the global minimum, the situation is even more interesting, as the articles mentioned above[4,13,44] all give a global minimum with four water molecules binding to the parent ion and one free O–H group, but in our work, 5 + 1_1 with five water molecules binding to the chloride ion and no free O–H group is the most stable isomer. Moreover, the predicted global minimum from the earlier literature[4,13,44] is actually found in our work as 4 + 2_1 for 0.4 kcal mol^{-1} higher energy. Although the energy difference is below the so-called *chemical accuracy*,[45] 5 + 1_1, which has more hydrogen bonds with the parent ion than 4 + 2_1, remains more convincing. However, with respect to the zero-point energy corrected energy, the energy order within the former five isomers changes significantly: 4 + 2_1 is the global minimum, while 5 + 1_2 changes from the fourth in total energy order without ZPE corrections to the second place, and 5 + 1_2 is slightly energetically higher than 4 + 2_1 with 0.08 kcal mol^{-1}. However, even with ZPE corrections, 5 + 1_1 remains highly competitive due to the very small energy difference of 0.27 kcal mol^{-1}.

B. Thermodynamics

The calculated thermodynamic parameters for $Cl^-(H_2O)_5$ and $Cl^-(H_2O)_6$ are given in Tables 1 and 2, respectively. The energy order change can be seen by comparing the binding energy at 0 K with the Gibbs free energy at 298.15 K, such as for 3 + 2_1 *versus* 3 + 2_2. This result could be explained by the effects of entropy, which is similar to the situation in the $Cl^-(H_2O)_n$ (n = 1–4) system.[2]

C. Vibrational frequencies

The vibrational frequency shifts for the former four structures of $Cl^-(H_2O)_5$ from DF-LMP2/aug′-cc-pVTZ are given in Table 3 in total energy order for comparison with the experimental values given by the Okumura group.[9]

As presented in Table 3, the shifts of the O–H stretching frequencies of chloride–water clusters are classified as follows: (1) nonbonded free [(O–H_f)], (2) hydrogen bonded to another water [(O–H_w)], and (3) hydrogen bonded to a chloride atom [(O–H_x)], as presented. In addition, the shifts caused by cooperative hydrogen bonding, as previously proposed, are given as [(O–H_c)].

Considering the large red shifts for ionic hydrogen bonds (IHB), an IHB is strengthened at the expense of weakening the hydrogen bonding between water molecules. Overall, the free O–H stretching frequencies remain nearly constant with respect to the corresponding mean value of the symmetric and asymmetric OH stretches in water (3886 cm^{-1}). In addition, for structures with free O–H group bonding, the largest red shift usually appears in the water molecular connecting to the free O–H group. Finally, the red shifts for the hydrogen-bonded O–H frequencies are much smaller than for the IHBs.

However, when examining the frequency shifts between the experimental and calculated values, as shown in Table 3, the high cluster temperature effects mentioned in the original experiment[9] would appear, which could be interpreted with

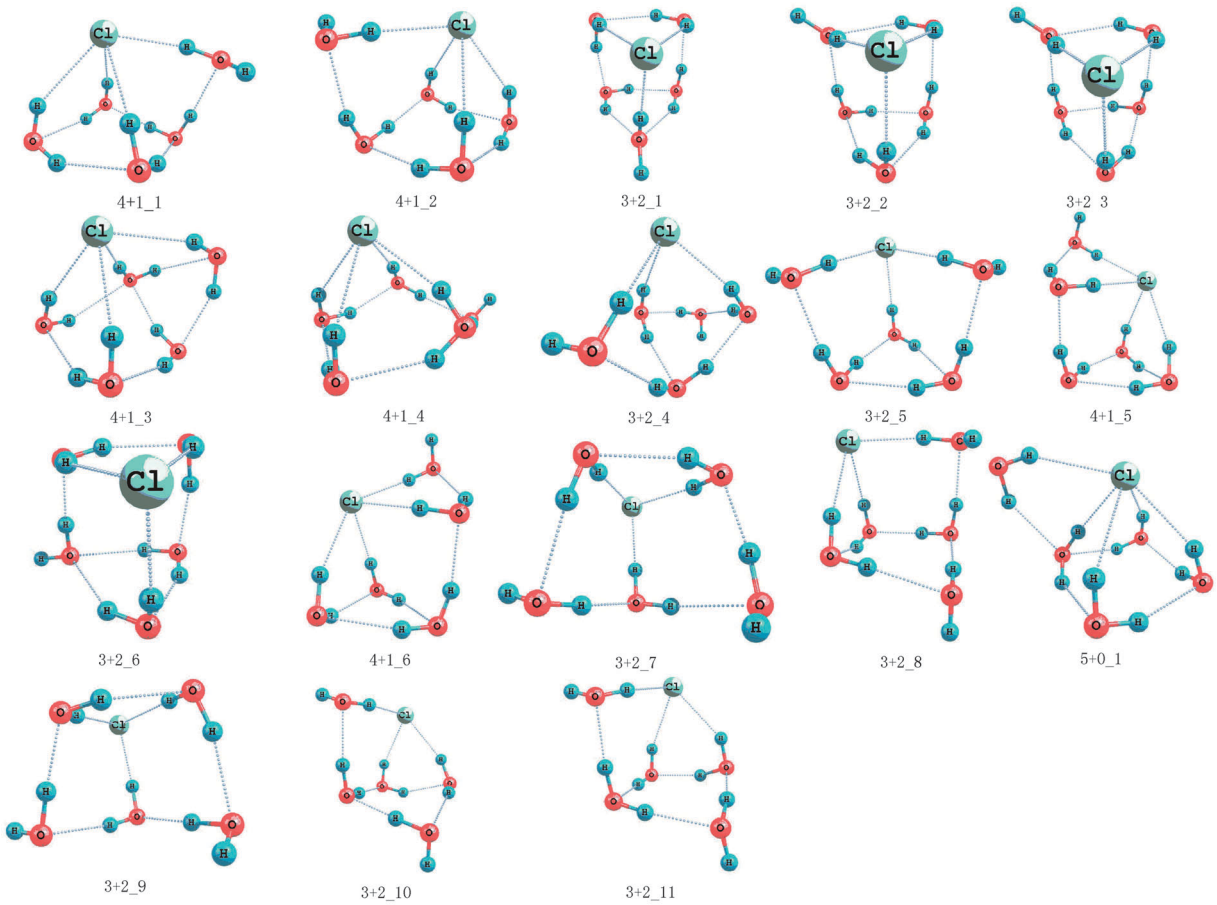

Fig. 1 The global minimum and the local minima for $Cl^-(H_2O)_5$ optimized at the DF-LMP2/aug′-cc-pVTZ level.

the aid of the temperature dependence of conformational populations. One point to be mentioned is that the order of these isomers in Table 3 was not arranged according to total energy at 0 K but by the Gibbs free energy at temperatures ranging from 100 K to 300 K, as shown in Fig. 5. The agreement between the experimental frequency shifts and the calculated ones follows the same order, which indicates that the cluster temperature under these experimental conditions could be in the range of 100 K to 400 K.

D. Temperature dependence of conformational population and Boltzmann averaged Gibbs free energy

The global minimum is important in that it has the greatest weight in the ensemble of energetically accessible conformers[45] at 0 K. However, as the systems grow larger and more complex, the energy differences between the global minimum and other local minima are becoming smaller, which is also caused by flexible hydrogen bonding, so including the contributions from all lower energy isomers might be important. In addition, temperature effects could also contribute to the stability order alternation of isomers. Thus, investigating the coupling effects of lower energy isomer contributions and temperature effects could provide a more accurate picture of the relative isomer stability.

Considering the Boltzmann distribution of the lower energy isomers, here we used the Boltzmann averaged Gibbs free energy to study the flatness of the potential energy surface of $Cl^-(H_2O)_n$ (n = 5–6). The equations are listed in follows:

$$\eta_n^i = \frac{e^{\frac{-\Delta\Delta G_n^i}{k_B T}}}{\sum_i e^{\frac{-\Delta\Delta G_n^i}{k_B T}}} \quad (10)$$

$$\Delta G_n = \sum_i \eta_n^i \Delta G_n^i \quad (11)$$

where

$$\Delta G_n^i = G_n^i - G^{Cl^-} - nG^W \quad (12)$$

$$\Delta\Delta G_n^i = \Delta G_n^i - \min\{\Delta G_n^i\} \quad (13)$$

Here n and i represent the number of water molecule in a cluster and the isomer order respectively. Cl^- and W are separately given for the abbreviation of chloride ion and water.

The conformational population depending on the temperature variance for $Cl^-(H_2O)_5$ and $Cl^-(H_2O)_6$ is shown in Fig. 3 and 4, respectively. Additionally, the conformational population of the most stable isomers for $Cl^-(H_2O)_n$ (n = 5–6) and the comparison between the Gibbs free energy and Boltzmann

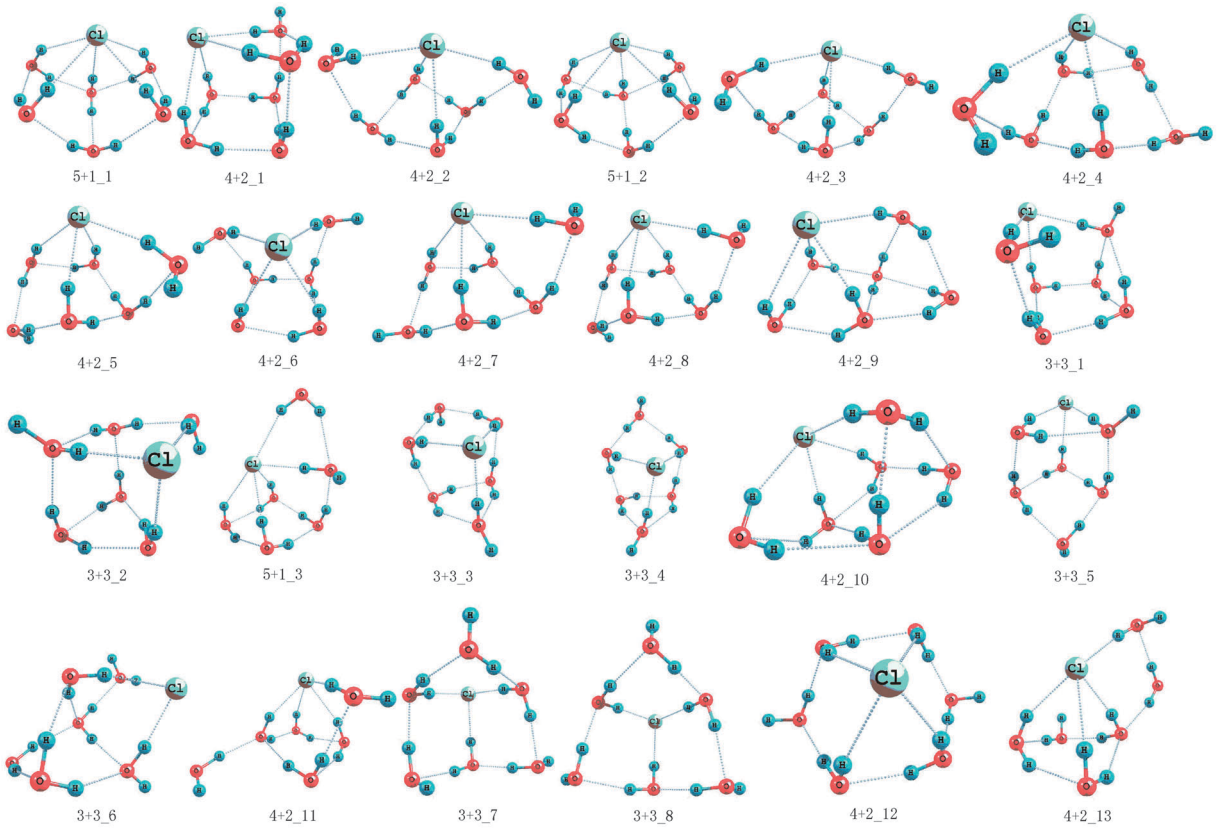

Fig. 2 The global minimum and the local minima for $Cl^-(H_2O)_6$ optimized at the DF-LMP2/aug′-cc-pVTZ level.

Table 2 Binding energies at 0 K (ΔE_e^{0K}), ZPE-corrected binding energies at 0 K (ΔE_0^{0K}), enthalpies at 298.15 K ($\Delta H^{298.15K}$), Gibbs free energy at 298.15 K ($\Delta G^{298.15K}$) for isomers of $Cl^-(H_2O)_6$ (in kcal mol^{-1})

Isomers	ΔE_e^{0K}	ΔE_0^{0K}	$\Delta H^{298.15K}$	$\Delta G^{298.15K}$
5 + 1_1	−81.65	−66.88	−68.12	−40.20
4 + 2_1	−81.25	−67.15	−67.36	−40.72
4 + 2_2	−81.09	−66.73	−68.45	−39.45
5 + 1_2	−80.93	−67.07	−67.60	−39.96
4 + 2_3	−80.86	−66.94	−68.27	−39.37
4 + 2_4	−80.07	−66.00	−67.44	−38.44
4 + 2_5	−79.93	−65.10	−67.32	−38.34
4 + 2_6	−79.80	−65.99	−67.27	−38.65
4 + 2_7	−79.68	−65.61	−67.19	−38.49
4 + 2_8	−79.54	−65.87	−67.06	−38.28
4 + 2_9	−79.45	−65.69	−65.51	−39.22
3 + 3_1	−79.39	−65.68	−66.96	−38.17
3 + 3_2	−79.34	−65.59	−66.86	−37.94
5 + 1_3	−79.09	−65.44	−66.64	−38.68
3 + 3_3	−79.04	−65.03	−66.60	−37.55
3 + 3_4	−78.97	−65.09	−66.54	−37.66
4 + 2_10	−78.88	−64.95	−66.25	−37.56
3 + 3_5	−78.82	−64.91	−66.41	−37.37
3 + 3_6	−78.40	−64.88	−66.73	−37.00
4 + 2_11	−78.27	−65.07	−66.42	−37.24
3 + 3_7	−78.22	−64.50	−66.46	−36.15
3 + 3_8	−78.14	−64.27	−66.37	−36.29
4 + 2_12	−78.11	−64.38	−65.62	−37.07
4 + 2_13	−77.80	−64.40	−65.99	−36.99

averaged Gibbs free energy are given in Tables 4 and 5 and Fig. 5. Considering that cluster dissociation might occur at a very high temperature, the conformational population with temperature more than 400 K is not given.

For both cases of $Cl^-(H_2O)_5$ and $Cl^-(H_2O)_6$ shown in Fig. 3 and 4, respectively, the weight of the global minimum according to total energy without ZPE correction decreases while the roles of other local minima become competitive as the temperature increases. However, the patterns of $Cl^-(H_2O)_n$ (n = 5–6) are significantly different due to their considerably different absolute and relative Gibbs free energy among the stable minima, which also reflects the different flatness of their potential energy surfaces.

For the case of $Cl^-(H_2O)_5$, as given in Fig. 3, the global minimum weighs more than any other local minima below a temperature of 350 K or so, but its leading role decreases thereafter. Near 350 K, three isomers, 4 + 1_2, 3 + 2_2 and 3 + 2_3, are very competitive toward the global minimum, and at temperatures above 350 K, the conformational populations of 4 + 1_1 and 4 + 1_2 both decrease while 3 + 2_2 and 3 + 2_3 increase. Moreover, the strong temperature effect could be seen in the less competitive role of 3 + 2_1, even though its total energy is quite close to the global minimum with an energy difference of 1.14 kcal mol^{-1}.

For the case of $Cl^-(H_2O)_6$ given in Fig. 4, below 200 K, the competitive local minimum, 4 + 2_1 has greater weight than 5 + 1_1 and increased in weight with increasing temperature. Another local minimum, 4 + 2_2, whose energy is only 0.56 kcal mol^{-1} higher than the global minimum in terms of total energy at 0 K, follows the same trend as 5 + 1_1.

Table 3 Comparison between DF-LMP2/aug′-cc-pVTZ predicted and experimentally determined vibrational frequency shifts for $Cl^-(H_2O)_5$ (in cm^{-1})

O–H stretch frequencies features for $Cl^-(H_2O)_5$	[(O–H_c)]	[(O–H_x)]	[(O–H_w)]	[(O–H_f)]	Total average shift differences
Experimental values	−474	−266	−159	−11	
4 + 1_1	−412	−221	−189	−19	
Shift differences	62	45	−30	−8	17.25
4 + 1_2	−449	−199	−149	−1	
Shift differences	25	67	10	10	28
3 + 2_2	−518	−317	−204	8	
Shift differences	−44	−51	−45	19	−30.25
3 + 2_1	−364	−185	−115	8	
Shift differences	110	81	44	19	63.5

The shifts are given with respect to the corresponding mean of the symmetric and symmetric OH stretch in water calculated in DF-LMP2/aug′-cc-pVTZ (3886 cm^{-1}) and the experimental shifts are given by the Okumura group.[9]

Comparing the conformational populations of isomers for $Cl^-(H_2O)_5$ at 50 K and 298.15 K shown in Table 4, we determined that differences between the Boltzmann averaged Gibbs free energy and the Gibbs free energy were increasing

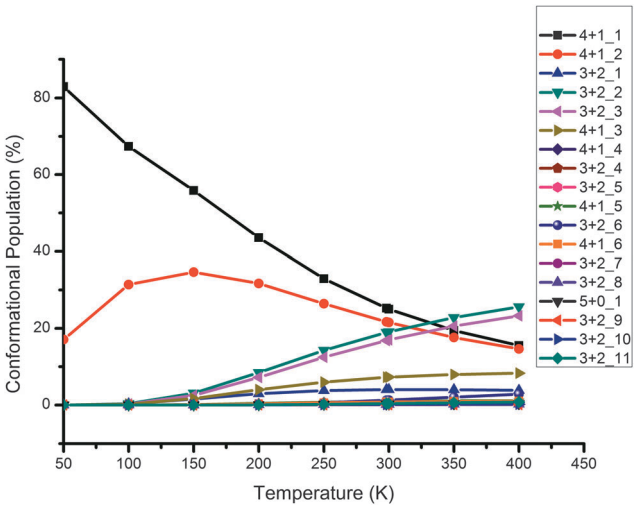

Fig. 3 The conformational population change for the low isomers of $Cl^-(H_2O)_5$ depending on the temperature variance.

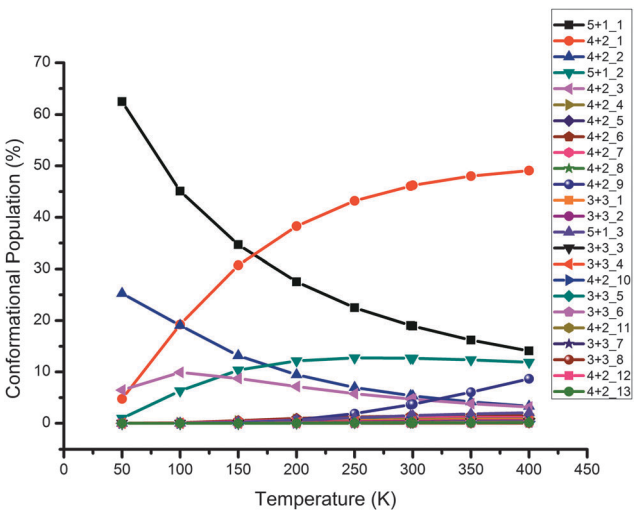

Fig. 4 The conformational population change for the low isomers of $Cl^-(H_2O)_6$ depending on the temperature variance.

Table 4 Conformational population (%) and Boltzmann averaged Gibbs free energy (kcal mol^{-1}) for the most stable isomers of $Cl^-(H_2O)_5$ at temperatures of 50 K, 100 K and 298.15 K

Temperature	Isomers	ΔG	Conformational population	Boltzmann averaged Gibbs free energy
50	4 + 1_1	−14.51	82.9	−14.49
	4 + 1_2	−14.36	17.1	
	3 + 2_1	−13.45	1.78479×10^{-03}	
	3 + 2_2	−13.36	7.13928×10^{-04}	
	3 + 2_3	−13.30	4.02573×10^{-04}	
100	4 + 1_1	−17.84	67.3	−17.78
	4 + 1_2	−17.69	31.4	
	3 + 2_1	−16.78	0.3	
	3 + 2_2	−16.81	0.4	
	3 + 2_3	−16.75	0.3	
298.15	4 + 1_1	−36.46	25.3	−36.14
	4 + 1_2	−36.37	21.7	
	3 + 2_1	−35.38	4.1	
	3 + 2_2	−36.29	18.9	
	3 + 2_3	−36.22	16.8	

Table 5 Conformational population (%) and Boltzmann averaged Gibbs free energy (kcal mol^{-1}) for the most stable isomers of $Cl^-(H_2O)_6$ at temperatures of 50 K, 100 K and 298.15 K

Temperature	Isomers	ΔG	Conformational population	Boltzmann averaged Gibbs free energy
50	5 + 1_1	−16.30	62.5	−16.24
	4 + 2_1	−16.04	4.8	
	4 + 2_2	−16.21	25.3	
	5 + 1_2	−15.88	1.0	
	4 + 2_3	−16.07	6.5	
100	5 + 1_1	−19.82	45.1	−19.70
	4 + 2_1	−19.65	19.2	
	4 + 2_2	−19.65	19.0	
	5 + 1_2	−19.43	6.3	
	4 + 2_3	−19.52	9.9	
298.15	5 + 1_1	−40.20	19.0	−40.14
	4 + 2_1	−40.72	46.1	
	4 + 2_2	−39.45	5.4	
	5 + 1_2	−39.96	12.7	
	4 + 2_3	−39.37	4.7	

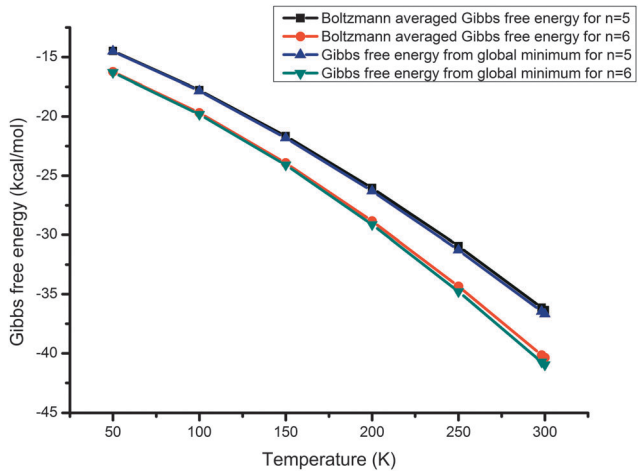

Fig. 5 The comparison between Boltzmann averaged Gibbs free energy and Gibbs free energy from global minimum $Cl^-(H_2O)_n$ (n = 5–6) depending on the temperature variance.

from 0.02 kcal mol^{-1} to 0.32 kcal mol^{-1}. For the case of $Cl^-(H_2O)_6$ shown in Table 5, the situation is quite similar, with the energy differences ranging from 0.06 kcal mol^{-1} to 0.58 kcal mol^{-1}. Thus, the higher number of predicted local minima as the systems of interest becomes larger and the higher conformational population of local minima other than the global one with increasing temperature necessitate the inclusion of Boltzmann averaging, especially for non-valance environments such as the chloride solvation systems in this article.

As shown in Fig. 5, the thermodynamic stability as calculated from the Boltzmann average and temperature effects has been considered. Compared to $Cl^-(H_2O)_5$, the consistent lower Gibbs free energy of $Cl^-(H_2O)_6$ at different temperature proves that the coupling consequence of various isomer contributions and temperature effects does not change the relative stability between $Cl^-(H_2O)_5$ and $Cl^-(H_2O)_6$. Moreover, after carefully investigating the magnitude caused by both effects, the temperature effects apparently contribute much more to the stability than the Boltzmann averaging.

E. Optical properties

For chloride ions, as the spherical case, the anisotropic polarizability $\Delta\alpha$ is zero, and correspondingly the depolarization ratios σ are all zero as the scattered light is completely polarized. When $\Delta\alpha \neq 0$, the scattered is no longer polarized and depolarization is represented by σ, which is the case for $Cl^-(H_2O)_n$ (n = 1–6).

It is shown that different isomers within clusters give very similar isotropic mean polarizabilities $\bar{\alpha}$ while the anisotropic polarizabilities $\Delta\alpha$ are very much isomer dependent, which has been observed in sulfuric acid hydration systems.[16] Additionally, the isotropic mean polarizabilities $\bar{\alpha}$ are quite size dependent and vary linearly with correlation coefficient ρ = 0.99986 as

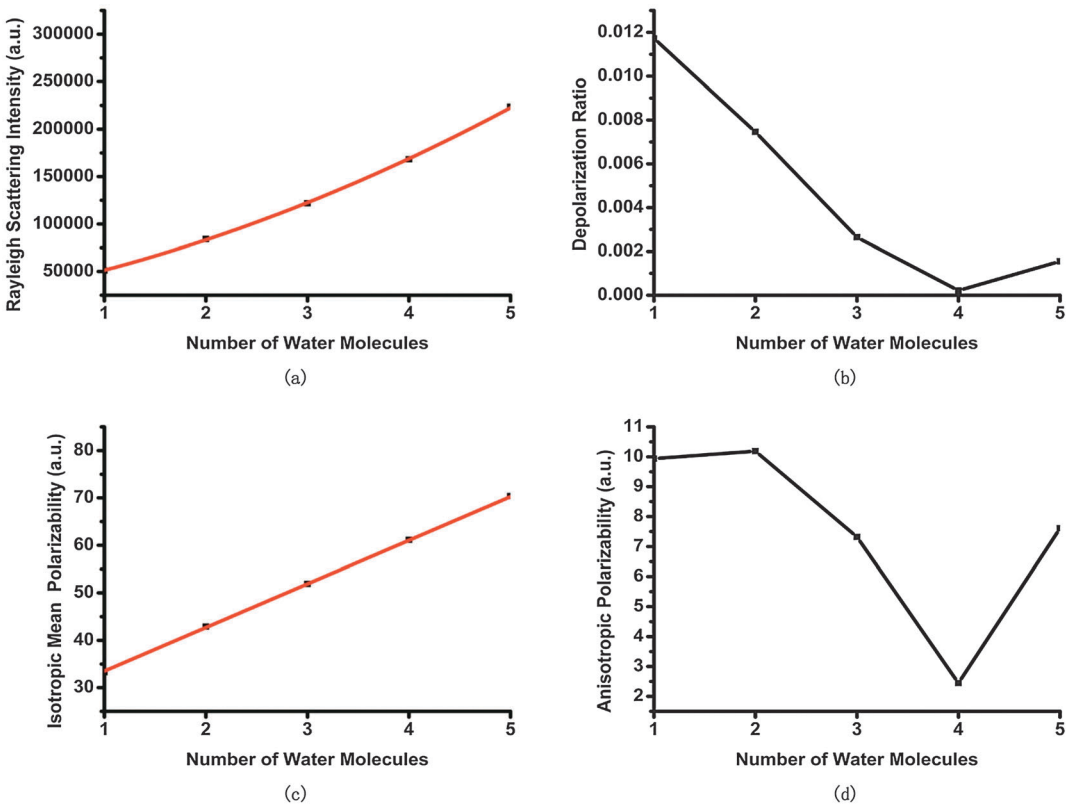

Fig. 6 The Rayleigh light scattering and cluster polarizability properties: (a) Rayleigh light scattering intensities as a function of water molecules; (b) depolarization ratio as a function of water molecules; (c) isotropic mean polarizabilities as a function of water molecules; (d) anisotropic polarizabilities as a function of water molecules.

Table 6 Depolarization ratios and Rayleigh scattering intensities for the perpendicular and parallel components of linear polarized light for chloride hydration systems calculated at the level of mp2/aug′-cc-pvdz

System	$\bar{\alpha}_{\mathrm{Binding}}$	$\Delta\alpha_{\mathrm{Binding}}$	σ_{p}	σ_{c}	$\Re_{\mathrm{p}\perp}$	$\Re_{\mathrm{p}\parallel}$
1 + 0	2.38	9.94	0.0059	0.0119	50519.35	592.46
2 + 0	3.83	10.19	0.0037	0.0075	83511.67	622.87
3 + 0	4.67	7.32	0.0013	0.0027	121553.20	321.43
4 + 0	5.76	2.45	0.0001	0.0002	168291.19	35.88
4 + 1_1	6.81	7.61	0.0008	0.0016	223208.63	347.36
3 + 2_1	7.14	7.60	0.0008	0.0015	225294.01	346.61
5 + 0_1	6.40	6.31	0.0005	0.0011	220462.07	239.19
5 + 1_1	7.50	6.45	0.0004	0.0009	282678.91	249.69

shown in Fig. 6(c), consistent with the study of methanol clusters.[46] Comparatively, it is observed that the anisotropic polarizability $\Delta\alpha$ show quite a different pattern as from a dimer to tetramer $\Delta\alpha$ decreases rapidly and then increases with a big step from a tetramer to pentamer. From Fig. 6(a) and (b), it is quite clearly observed that the Rayleigh light scattering intensity of natural light $\Re_n$ and the depolarization ratios σ_n is the function of the number of water molecules in the cluster. And the non-linear dependence of $\Re_n$ on the number of water molecules is shown to follow the trend of a second order polynomial with correlation coefficient ρ = 0.99988, consistent with the results of sulfuric acid hydration systems.[16] The calculated depolarization ratios σ_n are observed to rapidly decay as the cluster grows. This is due to an increase in the mean isotropic polarizability with the number of molecules in combination with the anisotropic polarizability being relatively constant in the range of 2–11 a.u. This is consistent with what is to be expected as the cluster change from a molecular cluster into a spherical isotropic particle.

From the previous studies[46,47] of Rayleigh scattering properties, the remarkable differences among different isomers have been observed, which indicate that $\Delta\alpha$ and σ could be alternative parameters to characterize different conformations. However, in our study, even though 4 + 1_1 and 3 + 2_1 show different bonding patterns with various Cl–H and O–H hydrogen bonding number, the $\Delta\alpha_{\mathrm{Binding}}$ difference between 4 + 1_1 and 3 + 2_1 is quite small, which is even smaller than that of $\bar{\alpha}_{\mathrm{Binding}}$ as shown in Table 6. For depolarization ratios, the case is similar. So at least for chloride ion hydration systems, the anisotropic polarizability and depolarization ratio cannot be regarded as the alternative parameters, which is similar to the case of methanol hydration systems.[37]

Inspired by the earlier research of investigation the relevance between hydrogen bonding number and cluster polarizability,[48] we have fitted the calculated isotropic mean polarizability values as a linear function of cluster size n, $\bar{n}_{\mathrm{Cl-H}}$ and $\bar{n}_{\mathrm{O-H}}$:

$$\bar{\alpha} = a + b \times n + c \times \bar{n}_{\mathrm{Cl-H}} + d \times \bar{n}_{\mathrm{O-H}} \qquad (14)$$

where $\bar{n}_{\mathrm{Cl-H}} = \frac{n_{\mathrm{Cl-H}}}{n}$ and $\bar{n}_{\mathrm{O-H}} = \frac{n_{\mathrm{O-H}}}{n}$ represent the average Cl–H hydrogen bonding number and O–H hydrogen bonding number respectively. The fit is found to be excellent with a correlation efficient as 0.9999. It indicates that the Cl–H hydrogen bonds and O–H hydrogen bonds both contribute to the cluster polarizability.

Conclusions

In this paper, BH coupled with the DFT method was employed to search for the global and local minima of $Cl^-(H_2O)_n$ (n = 5–6), while the benchmarked[2] method, DF-LMP2, was applied for the final geometry optimization and frequency calculations.

Structural and energetics analysis showed that the global minimum of $Cl^-(H_2O)_5$ agreed well with certain earlier literature reports,[13] and the appearance of a predicted global minimum from other articles[4,44] as a local minimum in our work further confirmed the validity of our predicted global minimum.

Thermodynamics analysis showed the energy of order alternation caused by the entropy effect, which has been observed in $Cl^-(H_2O)_n$ (n = 1–4), and vibrational properties analysis gave that free O–H group stretch frequency similar to the symmetric and asymmetric OH stretch in water. Moreover, the red shift of ion hydrogen bonding and hydrogen bonding within the water network was similar to the red shift of $Cl^-(H_2O)_n$ (n = 1–4).[2]

Incorporating the contributions of the lower energy minima by the Boltzmann averaged Gibbs free energy indicated the small role of lower energy isomers, aside from the global one, in the potential energy surface. However, the conformational population of these isomers shows various temperature-dependence characteristics that reflect the strong entropy effect of the chloride ion hydration systems. Moreover, the conformational population at a temperature which is close to that of the experiment, like the vibrational predissociation spectra experiment, might give more information to evaluate the degree of fitting between the simulated and the experiment results.

Finally, the Rayleigh scattering properties have been studied. It turns out that Rayleigh scattering intensities of natural light follow the second order polynomial trend with the cluster size increasing while the isotropic mean polarizabilities show a linear relation with the cluster size. Besides, the treatment of the anisotropic polarizability and depolarization ratio as structure characteristics must be carefully done as two isomers of $Cl^-(H_2O)_5$ give similar values.

Acknowledgements

The study was supported by grants from the National Natural Science Foundation of China (21133008) and ''Interdisciplinary and Cooperative Team'' of CAS. is also made to the ''Thousand Youth Talents Plan''. Part of the computation was performed at the Supercomputing Center of the Chinese Academy of Sciences and Supercomputing Center of USTC.

References

1 M. Schütz, H.-J. Werner, R. Lindh and F. R. Manby, *J. Chem. Phys.*, 2004, **121**, 737–750.
2 S. Jiang, Y. R. Liu, T. Huang, H. Wen, K. M. Xu, W. X. Zhao, W. J. Zhang and W. Huang, *J. Comput. Chem.*, 2014, **35**, 159–165.
3 J. Kim, H. M. Lee, S. B. Suh, D. Majumdar and K. S. Kim, *J. Chem. Phys.*, 2000, **113**, 5259–5272.

4 R. W. Gora, S. Roszak and J. Leszczynski, *Chem. Phys. Lett.*, 2000, **325**, 7–14.
5 M. Arshadi, R. Yamdagni and P. Kebarle, *J. Phys. Chem.*, 1970, **74**, 1475–1482.
6 K. Hiraoka, S. Mizuse and S. Yamabe, *J. Phys. Chem.*, 1988, **92**, 3943–3952.
7 P. Ayotte, G. H. Weddle and M. A. Johnson, *J. Chem. Phys.*, 1999, **110**, 7129–7132.
8 P. Ayotte, S. B. Nielsen, G. H. Weddle, M. A. Johnson and S. S. Xantheas, *J. Phys. Chem. A*, 1999, **103**, 10665–10669.
9 J.-H. Choi, K. T. Kuwata, Y.-B. Cao and M. Okumura, *J. Phys. Chem. A*, 1998, **102**, 503–507.
10 P. Ayotte, G. H. Weddle, J. Kim and M. A. Johnson, *J. Am. Chem. Soc.*, 1998, **120**, 12361–12362.
11 G. Markovich, S. Pollack, R. Giniger and O. Cheshnovsky, *J. Chem. Phys.*, 1994, **101**, 9344–9353.
12 D. Serxner, C. E. Dessent and M. A. Johnson, *J. Chem. Phys.*, 1996, **105**, 7231–7234.
13 H. M. Lee, D. Kim and K. S. Kim, *J. Chem. Phys.*, 2002, **116**, 5509–5520.
14 H. M. Lee and K. S. Kim, *J. Chem. Phys.*, 2001, **114**, 4461–4471.
15 A. B. Nadykto, F. Yu and A. Al Natsheh, *Int. J. Mol. Sci.*, 2009, **10**, 507–517.
16 J. Elm, P. Norman, M. Bilde and K. V. Mikkelsen, *Phys. Chem. Chem. Phys.*, 2014, **16**, 10883–10890.
17 T. L. Fonseca, M. A. Castro, B. J. Cabral, K. Coutinho and S. Canuto, *Chem. Phys. Lett.*, 2009, **481**, 73–77.
18 W. Chen, Z.-R. Li, D. Wu, F.-L. Gu, X.-Y. Hao, B.-Q. Wang, R.-J. Li and C.-C. Sun, *J. Chem. Phys.*, 2004, **121**, 10489–10494.
19 D. Deaven and K. Ho, *Phys. Rev. Lett.*, 1995, **75**, 288–291.
20 J. A. Niesse and H. R. Mayne, *J. Chem. Phys.*, 1996, **105**, 4700–4706.
21 J. Mestres and G. E. Scuseria, *J. Comput. Chem.*, 1995, **16**, 729–742.
22 S. Kirkpatrick, D. G. Jr. and M. P. Vecchi, *Science*, 1983, **220**, 671–680.
23 S. Goedecker, *J. Chem. Phys.*, 2004, **120**, 9911–9917.
24 D. J. Wales and J. P. Doye, *J. Phys. Chem. A*, 1997, **101**, 5111–5116.
25 S. G. Neogi and P. Chaudhury, *J. Comput. Chem.*, 2013, **34**, 471–491.
26 S. G. Neogi and P. Chaudhury, *J. Comput. Chem.*, 2012, **33**, 629–639.
27 B. Delley, *J. Chem. Phys.*, 1990, **92**, 508–517.
28 W. Huang, R. Pal, L.-M. Wang, X. C. Zeng and L.-S. Wang, *J. Chem. Phys.*, 2010, **132**, 054305.
29 W. Huang, H.-J. Zhai and L.-S. Wang, *J. Am. Chem. Soc.*, 2010, **132**, 4344–4351.
30 W. Huang and L.-S. Wang, *Phys. Rev. Lett.*, 2009, **102**, 153401.
31 W. Huang, M. Ji, C.-D. Dong, X. Gu, L.-M. Wang, X. G. Gong and L.-S. Wang, *ACS Nano*, 2008, **2**, 897–904.
32 W. Huang, A. P. Sergeeva, H.-J. Zhai, B. B. Averkiev, L.-S. Wang and A. I. Boldyrev, *Nat. Chem.*, 2010, **2**, 202–206.
33 L.-L. Yan, Y.-R. Liu, T. Huang, S. Jiang, H. Wen, Y.-B. Gai, W.-J. Zhang and W. Huang, *J. Chem. Phys.*, 2013, **139**, 244312.
34 H. Do and N. A. Besley, *J. Chem. Phys.*, 2012, **137**, 134106.
35 H. Do and N. A. Besley, *J. Phys. Chem. A*, 2013, **117**, 5385–5391.
36 Y.-R. Liu, H. Wen, T. Huang, X.-X. Lin, Y.-B. Gai, C.-J. Hu, W.-J. Zhang and W. Huang, *J. Phys. Chem. A*, 2013, **118**, 508–516.
37 E. E. Fileti, R. Rivelino and S. Canuto, *J. Phys. B: At., Mol. Opt. Phys.*, 2003, **36**, 399.
38 M. J. Frisch, G. W. Trucks, H. B. Schlegel, G. E. Scuseria, M. A. Robb, J. R. Cheeseman, G. Scalmani, V. Barone, B. Mennucci, G. A. Petersson, H. Nakatsuji, M. Caricato, X. Li, H. P. Hratchian, A. F. Izmaylov, J. Bloino, G. Zheng, J. L. Sonnenberg, M. Hada, M. Ehara, K. Toyota, R. Fukuda, J. Hasegawa, M. Ishida, T. Nakajima, Y. Honda, O. Kitao, H. Nakai, T. Vreven, J. A. Montgomery Jr., J. E. Peralta, F. Ogliaro, M. J. Bearpark, J. Heyd, E. N. Brothers, K. N. Kudin, V. N. Staroverov, R. Kobayashi, J. Normand, K. Raghavachari, A. P. Rendell, J. C. Burant, S. S. Iyengar, J. Tomasi, M. Cossi, N. Rega, N. J. Millam, M. Klene, J. E. Knox, J. B. Cross, V. Bakken, C. Adamo, J. Jaramillo, R. Gomperts, R. E. Stratmann, O. Yazyev, A. J. Austin, R. Cammi, C. Pomelli, J. W. Ochterski, R. L. Martin, K. Morokuma, V. G. Zakrzewski, G. A. Voth, P. Salvador, J. J. Dannenberg, S. Dapprich, A. D. Daniels, Ö. Farkas, J. B. Foresman, J. V. Ortiz, J. Cioslowski and D. J. Fox, *Gaussian 09, Revision A.02*, Gaussian Inc., Wallingford, CT, 2009.
39 H. J. Werner, P. J. Knowles, G. Knizia, F. R. Manby and M. Schütz, *Wiley Interdiscip. Rev.: Comput. Mol. Sci.*, 2012, **2**, 242–253.
40 H.-J. Werner, P. J. Knowles, G. Knizia, F. R. Manby, M. Schütz, P. Celani, T. Korona, R. Lindh, A. Mitrushenkov, G. Rauhut, K. R. Shamasundar, T. B. Adler, R. D. Amos, A. Bernhardsson, A. Berning, D. L. Cooper, M. J. O. Deegan, A. J. Dobbyn, F. Eckert, E. Goll, C. Hampel, A. Hesselmann, G. Hetzer, T. Hrenar, G. Jansen, C. Köppl, Y. Liu, A. W. Lloyd, R. A. Mata, A. J. May, S. J. McNicholas, W. Meyer, M. E. Mura, A. Nicklass, D. P. O'Neill, P. Palmieri, K. Pflüger, R. Pitzer, M. Reiher, T. Shiozaki, H. Stoll, A. J. Stone, R. Tarroni, T. Thorsteinsson, M. Wang and A. Wolf, *MOLPRO, version 2010.1, a package of ab initio programs*.
41 H.-J. Werner and K. Pflüger, *Annu. Rep. Comput. Chem.*, 2006, **2**, 53–80.
42 R. Polly, H.-J. Werner, F. R. Manby and P. J. Knowles, *Mol. Phys.*, 2004, **102**, 2311–2321.
43 S. F. Boys and F. d. Bernardi, *Mol. Phys.*, 1970, **19**, 553–566.
44 M. Masamura, *J. Phys. Chem. A*, 2002, **106**, 8925–8932.
45 D. C. Young, *Computational chemistry: A practical guide for applying techniques to real world problems*, Wiley Interscience, New York, 2001.
46 E. Orestes, P. Chaudhuri and S. Canuto, *Mol. Phys.*, 2012, **110**, 297–306.
47 P. Chaudhuri and S. Canuto, *THEOCHEM*, 2006, **760**, 15–20.
48 T. K. Ghanty and S. K. Ghosh, *J. Chem. Phys.*, 2003, **118**, 8547–8550.